Chapter 5

Flow in a thin plate, application to RTM and SRIM processes

RTM and SRIM processes usually involve thin molds filled by symmetric fiber mats where dispersion effects are important (2; 26; 33). Therefore this chapter firstly focuses on flows in thin filled cavities and then develops a dispersion model for media with specific symmetries. The transversely isotropic symmetry is deeper investigated. As reactive fluid are besides used in RTM and SRIM processes, examples of constitutive equations – namely the viscosity and the kinetic function – are specified. Finally the difference between moving front velocity and temperature front velocity is explained. Numerical results illustrate these considerations.

In order to simplify the notations, the fluid phase averaged velocity $\langle \underline{v}_f \rangle$, the intrinsic phase pressure $\langle P_f \rangle^f$, and the porosity ε_f are noted as $\underline{v}$, p and ε respectively in the following developments.

5.1 Flow in a thin porous plate

Let us first consider a thin porous plate of dimensions equal to $L > l \gg h > 0$ along the x, y and z axis respectively, as illustrated in Fig. 5.1.

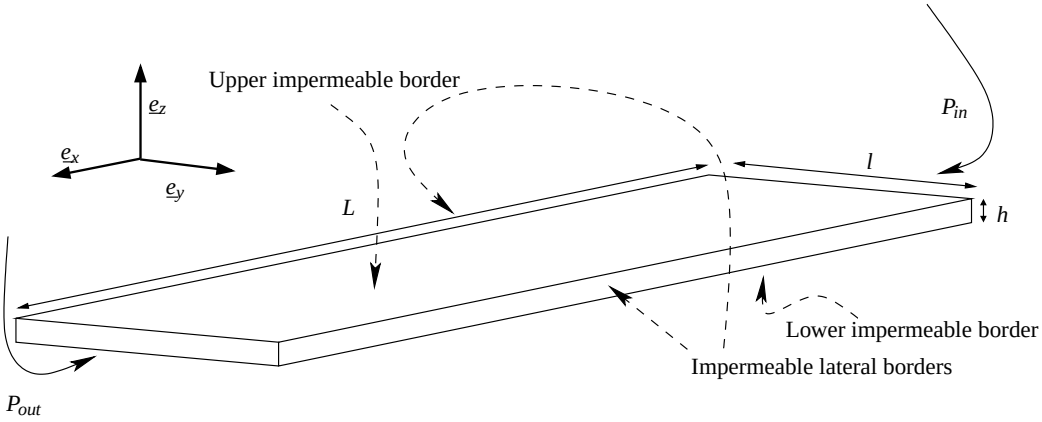

Figure 5.1: Scheme and dimensions of the thin porous plate. Sketch of the problem

We are interested in studying the solution of Darcy's equation by imposing a pressure gradient along the x axis and zero fluxes along the upper, lower and lateral borders. Let us first first focus on homogeneous media and show that the pressure field is in fact two-dimensional whereas the flow is uni-dimensional. It is then demonstrated that stratified porous media associated with anisotropic permeability generate a three dimensional flow whereas the pressure field remains two dimensional. Demonstrations are principally based on dimensional analysis.

5.1.1 Homogeneous media

For a non-isotropic medium, Darcy's equation and mass conservation write as :

$$\left\{ \begin{array}{rcl} \underline{v} & = & -\frac{1}{\varepsilon\eta}\underline{\underline{K}}\cdot\underline{\nabla}p \\ 0 & = & \underline{\nabla}\cdot\underline{v}\,. \end{array} \right. \tag{5.1.1}$$

Hence, including Darcy's equation in mass conservation provides the pressure equation :

$$0 = \underline{\nabla}\cdot\left(\frac{1}{\varepsilon\eta}\underline{\underline{K}}\cdot\underline{\nabla}p\right), \tag{5.1.2}$$

where the η and ε coefficients can be neglected in case of a homogeneous medium and a constant fluid viscosity.

At this point, it is useful to make the equation (5.1.2) non-dimensional. Therefore,

with use of the plate dimensions, the unknown first and second pressure derivatives are scaled as :

$$\left\{\begin{array}{rcl} \frac{\partial p}{\partial x} & \approx & \Delta p_x/L \\ \frac{\partial p}{\partial y} & \approx & \Delta p_y/l \\ \frac{\partial p}{\partial z} & \approx & \Delta p_z/h \\ \frac{\partial^2 p}{\partial_\triangle \partial_\triangledown} & \approx & min(\Delta p_\triangle, \Delta p_\triangledown)/l_\triangle l_\triangledown \quad \text{where } \triangle \text{ and } \triangledown \text{ represent } x, y \text{ or } z \end{array}\right. \tag{5.1.3}$$

Considering the imposed boundary conditions, we can assume that $\Delta p_x \gg \Delta p_y > \Delta p_z$. Equation (5.1.2) then scales as :

$$\left[K_{xx}\frac{\Delta p_x}{L^2} + K_{yy}\frac{\Delta p_y}{l^2} + K_{zz}\frac{\Delta p_z}{h^2} + 2K_{xy}\frac{\Delta p_y}{Ll} + 2K_{xz}\frac{\Delta p_z}{Lh} + 2K_{yz}\frac{\Delta p_z}{lh}\right] \cong 0. \tag{5.1.4}$$

The order of magnitude of Δp_z is chosen in such a way that the term divided by h^2 is of the same magnitude order as Δp_x, which provides :

$$K_{xx}\frac{\Delta p_x}{L^2} \approx K_{zz}\frac{\Delta p_z}{h^2} \tag{5.1.5}$$

or, in other words

$$\Delta p_x \approx \mathscr{O}\left(\frac{K_{zz}}{K_{xx}}\frac{L^2}{h^2}\right)\Delta p_z. \tag{5.1.6}$$

Since $L \gg h$ and assuming that $K_{zz} \approx K_{xx}$, it follows that :

$$\Delta p_x \gg \Delta p_z. \tag{5.1.7}$$

This short analysis shows that pressure variations along the z axis can be neglected in front of pressure variations along the x axis. The same conclusion can be drawn for the pressure variations along the y axis. Hence, the pressure essentially depends on x and y :

$$p = p(x,y). \tag{5.1.8}$$

Therefore, on the one hand this observation leads us to compute averaged equations across the z axis. Defining the gap-average of a field a by :

$$\bar{a} = \frac{1}{h}\int_0^h a\,dz\,, \tag{5.1.9}$$

Darcy's equation is rewritten for a homogeneous medium as :

$$\overline{\underline{v}} = \frac{1}{h}\int_0^h \underline{v}\,dz = -\frac{1}{h}\int_0^h \frac{1}{\varepsilon\eta}\underline{\underline{K}}\cdot\underline{\nabla}p\,dz = --\frac{1}{h}\int_0^h \frac{1}{\varepsilon\eta}\underline{\underline{K}}\,dz\cdot\underline{\nabla}p = -\frac{1}{\varepsilon\eta}\overline{\underline{\underline{K}}}\cdot\underline{\nabla}p\,, \tag{5.1.10}$$

while mass conservation writes as :

$$\underline{\nabla}\cdot\overline{\underline{v}} = 0\,. \tag{5.1.11}$$

Attention must be paid to the meaning of these variables. Indeed, they correspond to a higher level of averaging since they are averages of ensemble-averaged variables. Moreover, taking into account the gap-averaged mass equation (5.1.11) and the flux boundary conditions, it appears that the gap-averaged velocity is aligned with the lateral borders of the medium (along x axis), whatever the permeability tensor is.

On the other hand, the pressure field can easily be solved. Indeed, the gap-averaged Darcy equation (5.1.10) gives :

$$\overline{K}_{xx}\frac{\partial^2 p}{\partial^2 x}+2\overline{K}_{xy}\frac{\partial^2 p}{\partial x\partial y}+\overline{K}_{yy}\frac{\partial^2 p}{\partial^2 y}=0. \tag{5.1.12}$$

A linear field satisfies this equation and the pressure field is then equal to :

$$p=ax+by+c\,. \tag{5.1.13}$$

This solution is valid everywhere except near the inlet and outlet boundaries where an adaptation of this linear solution to the detailed pressure boundary conditions must take place. Considering the flux lateral boundary conditions, the relation between a and b can be determined. The flux indeed vanishes on the mold lateral borders, which provides the relations $v_y(0)=v_y(l)=-\frac{(K_{xy}a+K_{yy}b)}{\eta\varepsilon}=0$ and finally $\frac{a}{b}=-\frac{K_{yy}}{K_{yx}}$.

5.1.2 Stratified media

Previous considerations enable us to study the flow through a stratified medium, which consists in a superposition of various homogeneous layers (Fig. 5.2), such as for example a set of differently oriented fiber mats. In this section, we illustrate that the flow through this kind of medium can exhibit mass transfer between the layers due to the relative properties of each medium.

Each layer is characterized by its own permeability. As a particular case, we consider a two-layered medium with symmetric permeabilities :

$$[K_{ij}]=\begin{bmatrix}K_{xx} & K_{xy} & 0\\ K_{xy} & K_{yy} & 0\\ 0 & 0 & K_{zz}\end{bmatrix} \quad \text{for} \quad 0\le z\le h/2 \tag{5.1.14}$$

and

$$[K_{ij}]=\begin{bmatrix}K_{xx} & -K_{xy} & 0\\ -K_{xy} & K_{yy} & 0\\ 0 & 0 & K_{zz}\end{bmatrix} \quad \text{for} \quad h/2<z\le h. \tag{5.1.15}$$

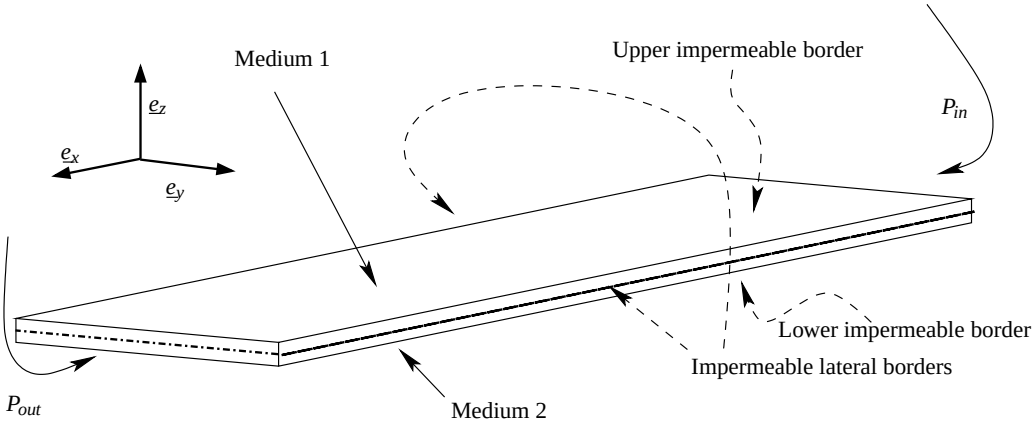

Figure 5.2: Scheme of a thin stratified porous plate with two layers. Sketch of the problem

This configuration corresponds to a pair of symmetric mats with respect to the *xz* plane. The gap-averaged permeability is equal to :

$$\left[\overline{K}_{ij}\right] = \begin{bmatrix} K_{xx} & 0 & 0 \\ 0 & K_{yy} & 0 \\ 0 & 0 & K_{zz} \end{bmatrix}. \tag{5.1.16}$$

Hence, solving Eq. (5.1.12) provides the pressure field, which is equal to :

$$p = a\,x + c. \tag{5.1.17}$$

Moreover, the gap-averaged velocity is as previously parallel to the plate lateral borders, contrarily to the detailed velocities in each layer which are not parallel to these borders. Indeed, introducing the pressure field (5.1.17) in the Darcy equation (5.1.1) gives :

$$\begin{cases} v_x &= -K_{xx}\,a/\varepsilon\eta \\ v_y &= -K_{xy}\,a/\varepsilon\eta \end{cases} \text{ for the upper layer } (0 \le z \le h/2), \tag{5.1.18}$$

and

$$\begin{cases} v_x &= -K_{xx}\,a/\varepsilon\eta \\ v_y &= K_{xy}\,a/\varepsilon\eta \end{cases} \text{ for the lower layer } (h/2 < z \le h). \tag{5.1.19}$$

These local velocities and the no flux lateral boundary conditions give evidence to the existence of some mass transfer across the two layers, which therefore results in 3D path-lines (Fig. 5.3). In fact, this 3D effect is present when non-isotropic layers are

used. It should be noted that this mass transfer becomes quite complex when more than two layers are superposed. A similar effect takes place along the flow front(s) (where it plays the same role as fountain flow in classical injection moulding) (51). However, this anisotropic effect is not the only origin of mass exchanges between the

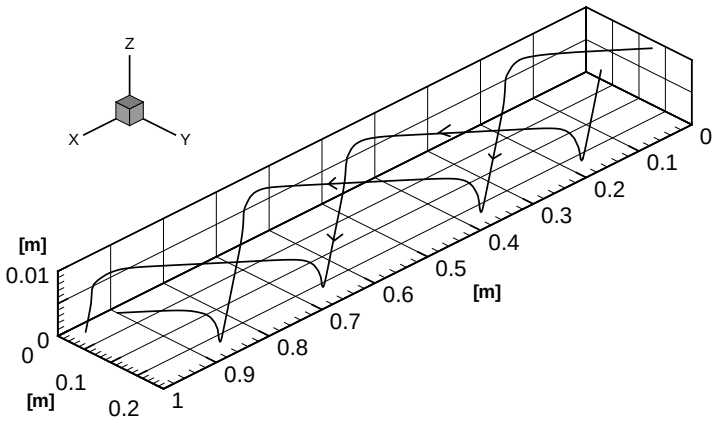

Figure 5.3: Path-lines of two selected material points through a 2-layered porous medium.

layers as is shown in the next section.

5.2 Permeability and dispersion in a transversely isotropic medium. Application to a thin stratified plate.

Hydrodynamic dispersion represents a second origin of mass transfer between the layers in the previous problem. In order to visualize this effect, let us consider a flow which consists in initially superposing and then continually injecting a given marking species into the lower and the upper layers at constant concentrations $c^{(1)}$ and $c^{(2)}$ (typically two different fluid colours can be used for this purpose). An enhancement of species diffusion between the layers will be observed as a consequence of the hydrodynamic dispersion effect which can be, or not, isotropic. This effect competes with the mass transfer taking place in the cavity lateral boundary layers. The objectives of this section are first to detail the modelling of transversely isotropic media and then to analyse the respective roles of mat anisotropy and hydrodynamic dispersion (whether or not isotropic) for our particular problem of a thin two-layered stratified plate.

5.2.1 Modelling of transversely isotropic media

In order to describe the medium, its permeability and hydrodynamic dispersion tensors have to be defined. These material properties depend on the geometry of the pores, their inter-connections and hence the global solid matrix structure.

This section is essentially related to tensorial analysis. Indeed, whereas permeability is classically represented by a second-order tensor, it should be recalled that hydrodynamic dispersion is expected to be better represented by a fourth-order tensor (Chapter 1). We will determine the minimum number of parameters necessary to describe isotropic and transversely isotropic media, for a second- and fourth-order tensor, taking into account the specific symmetries of permeability and hydrodynamic dispersion.

Second-order tensor : application to permeability

The general form of a second order tensor in the vector basis $\underline{e}_i$ is :

$$\underline{\underline{K}} = K_{ij}\, \underline{e}_i \underline{e}_j \ , \tag{5.2.20}$$

where the classical summation convention over repeated indices is used.

In the **isotropic** case, it can be demonstrated (52) that the second-order tensor basis is constituted by a single element, $\delta_{ij}\ \underline{e}_i \underline{e}_j$, where δ_{ij} is the Kronecker symbol. The general expression of isotropic second-order tensor components is then :

$$K_{ij} = K\ \delta_{ij} \ . \tag{5.2.21}$$

In some cases, the second-order tensor must be semi-positive definite (s.p.d.). A tensor exhibits this property if it satisfies the following inequality :

$$\underline{u} \cdot \underline{\underline{K}} \cdot \underline{u} \geq 0, \quad \forall \underline{u} \ . \tag{5.2.22}$$

It is easy to show that this property is ensured by the condition $K \geq 0$ when the tensor is isotropic.

A **transversely isotropic** medium is characterized by a principal direction with respect to which all perpendicular planes exhibit an isotropic character. Let us represent this normed direction by the symbol $\underline{l}$. The basis of second-order transversely isotropic tensors is then constituted by two independent elements (52), for example $l_i l_j$ and $\delta_{ij} - l_i l_j$. The general form of the second-order tensor components is then :

$$K_{ij} = K_{\parallel}\ l_i l_j + K_{\perp}\ (\delta_{ij} - l_i l_j) \, . \tag{5.2.23}$$

In order to illustrate these notations, let us align the basis vector $\underline{e}_1$ with $\underline{L}$. In this case, the tensor components write as :

$$[K_{ij}] = \begin{bmatrix} K_{\parallel} & 0 & 0 \\ 0 & K_{\perp} & 0 \\ 0 & 0 & K_{\perp} \end{bmatrix}, \tag{5.2.24}$$

and the notation becomes clear.

The s.p.d. character of the tensor is ensured by the inequalities

$$K_{\parallel} \geq 0 \quad \text{and} \quad K_{\perp} \geq 0. \tag{5.2.25}$$

Indeed Eq. (5.2.22) becomes in this case :

$$\underline{u} \cdot \underline{\underline{K}} \cdot \underline{u} = K_{\parallel} \left(\underline{L} \cdot \underline{u}\right)^2 + K_{\perp} \left(\underline{u} \cdot \underline{u} - \left(\underline{L} \cdot \underline{u}\right)^2\right) \geq 0\,, \quad \forall \underline{u}\,. \tag{5.2.26}$$

Since $\underline{u} \cdot \underline{u} - \left(\underline{L} \cdot \underline{u}\right)^2 > 0$ by Pythagore's theorem, the inequalities (5.2.25) are easily retrieved.

Fourth-order tensor : application to hydrodynamic dispersion

General 4$^{\text{th}}$-tensors are characterized by 81 ($= 3^4$) components. Nevertheless, since we are here interested in particular applications for symmetric media, it is shown in this section that the number of necessary components will be strongly reduced.

First of all let us recall that the 4$^{\text{th}}$-order hydrodynamic dispersion tensor has been introduced in order to model the dispersion effect in the energy and species conservation equations and possibly in the momentum conservation equation. Eq. (1.6.92) induces some symmetries :

$$\underline{\underline{D}}^D = \underline{\underline{\underline{L}}} : \frac{\langle \underline{v}_f \rangle \langle \underline{v}_f \rangle}{\| \langle \underline{v}_f \rangle \|} \quad \Longrightarrow \quad L_{ijkl} = L_{jikl} = L_{ijlk}. \tag{5.2.27}$$

The first symmetry is due to the symmetry of the dispersion tensor $\underline{\underline{D}}^D$, as related to the effective thermal and species dispersions governed by Eqs. (1.6.90) and (1.7.102), which are symmetric. The second symmetry is due to the selected velocity dependence for $\underline{\underline{D}}^D$.

In the **isotropic** case, a 4$^{\text{th}}$-order tensor is defined by 3 independent parameters (52) :

$$L_{ijkl} = \lambda\ \delta_{ij}\delta_{kl}\ +\ \frac{\mu}{2}\left(\delta_{ik}\delta_{jl}\ +\ \delta_{il}\delta_{jk}\right)\ +\ \frac{\nu}{2}\left(\delta_{ik}\delta_{jl}\ -\ \delta_{il}\delta_{jk}\right) \tag{5.2.28}$$

Nevertheless, the symmetries (5.2.27) induce that ν is zero. Hence only two parameters are necessary and the tensor is rewritten as :

$$L_{ijkl} = \lambda\ \delta_{ij}\delta_{kl}\ +\ \frac{\mu}{2}\left(\delta_{ik}\delta_{jl}\ +\ \delta_{il}\delta_{jk}\right). \tag{5.2.29}$$

Noting

$$\begin{array}{rcl} \lambda & = & L_\perp \\ \mu & = & L_\parallel - L_\perp, \end{array} \tag{5.2.30}$$

the dispersion tensor components are written as :

$$D^D_{ij} = L_\perp\ \delta_{ij}\|\underline{v}\| + \left(L_\parallel - L_\perp\right)\ \frac{v_i\ v_j}{\|\underline{v}\|}. \tag{5.2.31}$$

Analyzing this formulation when the flow in aligned with the medium principal direction allows us to understand the meaning of the used symbols. For example, for a velocity aligned along $\underline{e}_1$ ($\underline{v} = (v,0,0)$), the dispersion tensor writes as :

$$\left[D^D_{ij}\right] = \left[\begin{array}{ccc} L_\parallel v & 0 & 0 \\ 0 & L_\perp v & 0 \\ 0 & 0 & L_\perp v \end{array}\right]. \tag{5.2.32}$$

Another important character of this tensor relies on the fact that $\underline{\underline{D}}^D$ must be s.p.d.. Hence as previously, the following inequality must be satisfied :

$$\underline{u}\cdot\underline{\underline{D}}^D\cdot\underline{u} = \underline{u}\cdot\left(\underline{\underline{L}} : \frac{\underline{v}\,\underline{v}}{\|\underline{v}\|}\right)\cdot\underline{u} \geq 0,\ \forall \underline{u},\underline{v}. \tag{5.2.33}$$

It is shown in Annexe D that

$$L_\parallel \geq 0 \text{ et } L_\perp \geq 0 \tag{5.2.34}$$

is a necessary and sufficient condition to verify this semi-positive definiteness condition.

The **transversely isotropic** case involves more complex calculations which can be found in Annexe D. First of all, the basis of $\underline{\underline{L}}$ components is composed of 20 elements (52) :

- $l_i l_j l_k l_l$,
- $l_i l_j \delta_{kl}$, $l_i l_l \delta_{jk}$, $l_j l_k \delta_{il}$, $l_i l_k \delta_{jl}$, $l_j l_l \delta_{ik}$, $l_k l_l \delta_{ij}$, $l_j l_i \delta_{kl}$, $l_l l_i \delta_{jk}$, $l_k l_j \delta_{il}$, $l_k l_i \delta_{jl}$, $l_l l_j \delta_{ik}$, $l_l l_k \delta_{ij}$,
- $\delta_{ij}\delta_{kl}$, $\delta_{ik}\delta_{jl}$, $\delta_{il}\delta_{jk}$,
- $\varepsilon_{ijk} l_l$, $\varepsilon_{ijl} l_k$, $\varepsilon_{ikl} l_j$, $\varepsilon_{jkl} l_i$, (where ε_{ijk} is the classical permutation pseudo-tensor).

Taking into account the symmetries (5.2.27) of $\underline{\underline{L}}$, there are only six elements left :

- $l_i l_j l_k l_l$,
- $l_i l_j \delta_{kl}$
- $l_k l_l \delta_{ij}$,
- $\delta_{ij}\delta_{kl}$,
- $\delta_{ik}\delta_{jl} + \delta_{il}\delta_{jk}$,
- $l_i l_l \delta_{jk} + l_j l_k \delta_{il} + l_i l_k \delta_{jl} + l_j l_l \delta_{ik}$,

and the hydrodynamic dispersion tensor components can be rewritten as :

$$\begin{aligned} L_{ijkl} \;=\; & L_{\parallel\parallel}\, l_i l_j l_k l_l \\ & + L_{\parallel\perp}\, l_i l_j \left(\delta_{kl} - l_k l_l\right) \\ & + L_{\perp\parallel}\, \left(\delta_{ij} - l_i l_j\right) l_k l_l \\ & + L_{\perp\vdash} \left(\delta_{ij} - l_i l_j\right)\left(\delta_{kl} - l_k l_l\right) \\ & + \tfrac{1}{2}\left(L_{\perp\perp} - L_{\perp\vdash}\right) \left[\left(\delta_{ik} - l_i l_k\right)\left(\delta_{jl} - l_j l_l\right) + \left(\delta_{il} - l_i l_l\right)\left(\delta_{jk} - l_j l_k\right)\right] \\ & + L_{\bowtie} \left[l_i l_k(\delta_{jl} - l_j l_l) + l_j l_k(\delta_{il} - l_i l_l) + l_i l_l(\delta_{jk} - l_j l_k) + l_j l_l(\delta_{ik} - l_i l_k)\right]. \end{aligned} \tag{5.2.35}$$

The significance of each parameter can be understood by considering the basis vector $\underline{e}_1$ as aligned with the medium principal direction $\underline{l}$ and the velocity field successively aligned with $\underline{e}_1$, $\underline{e}_2$ and $\underline{e}_3$. The first symbol in L_{**} is related to the medium symmetry direction while the second symbol is related to flow direction.

Finally the s.p.d. character of $\underline{\underline{D}}^D$ is ensured by the following inequalities (Annexe D) :

$$L_{\parallel\parallel}, L_{\parallel\perp}, L_{\perp\parallel}, L_{\perp\vdash}, L_{\perp\perp} \geq 0 \quad \text{and} \quad 2\,|L_{\bowtie}| \leq \sqrt{L_{\parallel\parallel} L_{\perp\perp}} + \sqrt{L_{\parallel\perp} L_{\perp\parallel}}. \tag{5.2.36}$$

5.2.2 Mass transfer : competition between dispersion and mass transfer

In this section, we illustrate the competition between dispersion and mass transfer effects. Numerical results were computed by means of a code based on the algorithm described in the previous chapter. We again consider the flow through a thin stratified cavity (Fig. 5.2) of dimensions $1\,\mathrm{m} \times 0.2\,\mathrm{m} \times 0.01\,\mathrm{m}$, whose layers are each of $5\,\mathrm{mm}$ thickness. Inlet and outlet pressures are $1.05\,\mathrm{bar}$ and $1\,\mathrm{bar}$, while the constant resin

viscosity is $0.2\,\mathrm{kg\ m^{-1}\ s^{-1}}$. The lower and upper initial and inlet relative concentrations are $c^{(1)} = 0.25$ and $c^{(2)} = 0.75$ (Fig. 5.4). The porosity is 0.86 for both layers, which are assumed to be transversely isotropic.

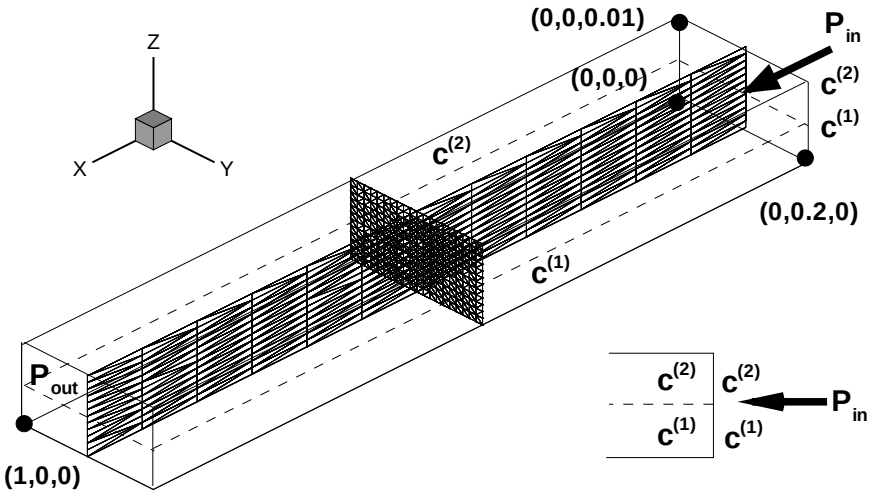

Figure 5.4: Sketch of the problem and cross-sections of the mesh for $x = 0.5\,\mathrm{m}$ and $y = 0.1\,\mathrm{m}$.

The principal permeabilities are $K_\perp = 10^{-8}\,\mathrm{m}^2$ and $K_\parallel = 10^{-7}\,\mathrm{m}^2$, while the larger permeability direction L (associated with the fiber orientation) is parallel to the mid-surface of the cavity and oriented in the upper and lower layers at -45° and 45° with respect to the average velocity $\overline{\langle v_f \rangle}$. Therefore, the permeability tensor writes as

$$K_{ij} = K_\parallel\, l_i l_j + K_\perp\,(\delta_{ij} - l_i l_j)\,, \tag{5.2.37}$$

with (l_i) given in the lower and upper layers by

$$\begin{cases} (l_i) = (l_i^{(1)}) = (\frac{\sqrt{2}}{2}, \frac{\sqrt{2}}{2}, 0), \\ (l_i) = (l_i^{(2)}) = (\frac{\sqrt{2}}{2}, -\frac{\sqrt{2}}{2}, 0). \end{cases} \tag{5.2.38}$$

The 3D mass transfer has been explained in the previous section and is illustrated in Figs. 5.3, 5.5 and 5.6.

In order to investigate the hydrodynamic dispersion effect and its competition with mass transfer, a coefficient $L = 0.17\,\mathrm{mm}$ has been used to represent the order of mag-

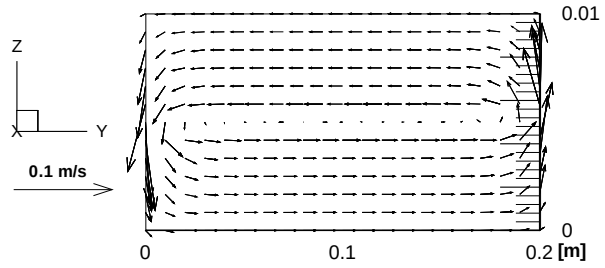

Figure 5.5: Cross-section of the velocity field for $x = 0.5\,\mathrm{m}$.

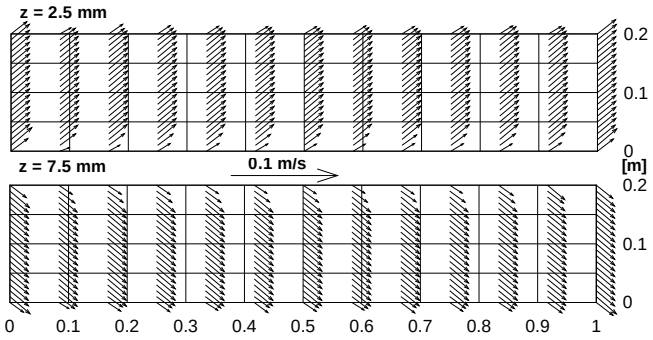

Figure 5.6: Cross-sections of the velocity field for $z = 2.5\,\mathrm{mm}$ and $z = 7.5\,\mathrm{mm}$.

nitude of the tensor L_{ijkl}. This rather high value as compared to the estimates provided by Mal et al. (26) was selected in order to enhance this effect in the simulations.

Several simulations were performed with different values of the dispersion tensor L_{ijkl}. Isotropic dispersion was first tested with $L_{\parallel} = L_{\perp} = L$. Subsequently, a transversely isotropic dispersion was investigated by setting to 0 chosen dispersion coefficients ($L_{\parallel\parallel}$, $L_{\parallel\perp}$, $L_{\perp\perp}$ ...) (Figs. 5.7 and 5.8). From these numerical experiments, we have observed that a significant role is played by $L_{\perp\parallel}$ only. This can be demonstrated by a detailed analysis of this particular problem.

On Figs. 5.7 and 5.8, it appears that, when the $L_{\perp\parallel}$ dispersion parameter is increased, the dispersion effect becomes more and more important and finally dominates the mass transfer effect (Fig. 5.7). In this latter case, the mass transfer has no time to occur while the dispersion phenomena can take place. In the other limiting case, i.e.

when no diffusion and dispersion effects take place, by considering the mass transfer effect and the flow pathlines, it appears that the generated flow can be compared to a pair of rotating together screws (Fig. 5.8).

In conclusion, it appears that complex transfer effects are generated (i) by a jointly non-uniform and non-isotropic permeability, and (ii) by a non-isotropic mechanical dispersion. Our program allows us to analyse this effect. However, it should be recalled on the one hand that, in order to deal with transport-dominated problems, accurate solution techniques must be set up and on the other hand that there remains a serious lack of experimental comparison in order to validate our dispersion model (even if first comparisons were shown in Chapter 3).

5.3 Reactive processes

In the Resin Transfer Molding (RTM) and Structural Reaction Injection Molding (SRIM) processes, the reactive resins are usually complex mixtures of several different species (in opposition to thermoplastics injection processes). Whereas thermoset injection molding (RTM) refers to heat activated resin (such as epoxy or unsaturated polyester) in a hot cavity where it undergoes solidification by a cross-linking mechanism (53), reaction injection molding (SRIM) refers to the injection of a low viscosity mixing-activated resin (such as polyurethane) in a moderately hot cavity, where it undergoes very fast solidification by a (generally) linear polymerization reaction (54). In the sequel, we use "reactive molding" without distinction for both processes.

As the mixture is usually composed of several species, additional species conservation equations including the appropriate reaction kinetics are necessary in order to rigorously model the reaction mechanisms. The parameters governing these sometimes numerous reactions are needed but are not always known. A cruder but simpler approach therefore consists in lumping all the information on the evolution of the different reactions into a single field called the degree of conversion. During polymerization, this quantity is advected with the injected resin and monotonically increases from 0 (no reaction having taken place) to a maximum value (1 when the resin has fully reacted). This approach nevertheless needs an accurate definition and kinetics for the degree of conversion. The governing equation writes as :

$$\frac{Dc}{Dt} = f_c(\cdot), \tag{5.3.39}$$

where the $D\cdot/Dt$ denotes material derivation and f_c is the overall reaction kinetics. The last equation is of course a simplified form of Eq. (1.7.103). The degree of con-

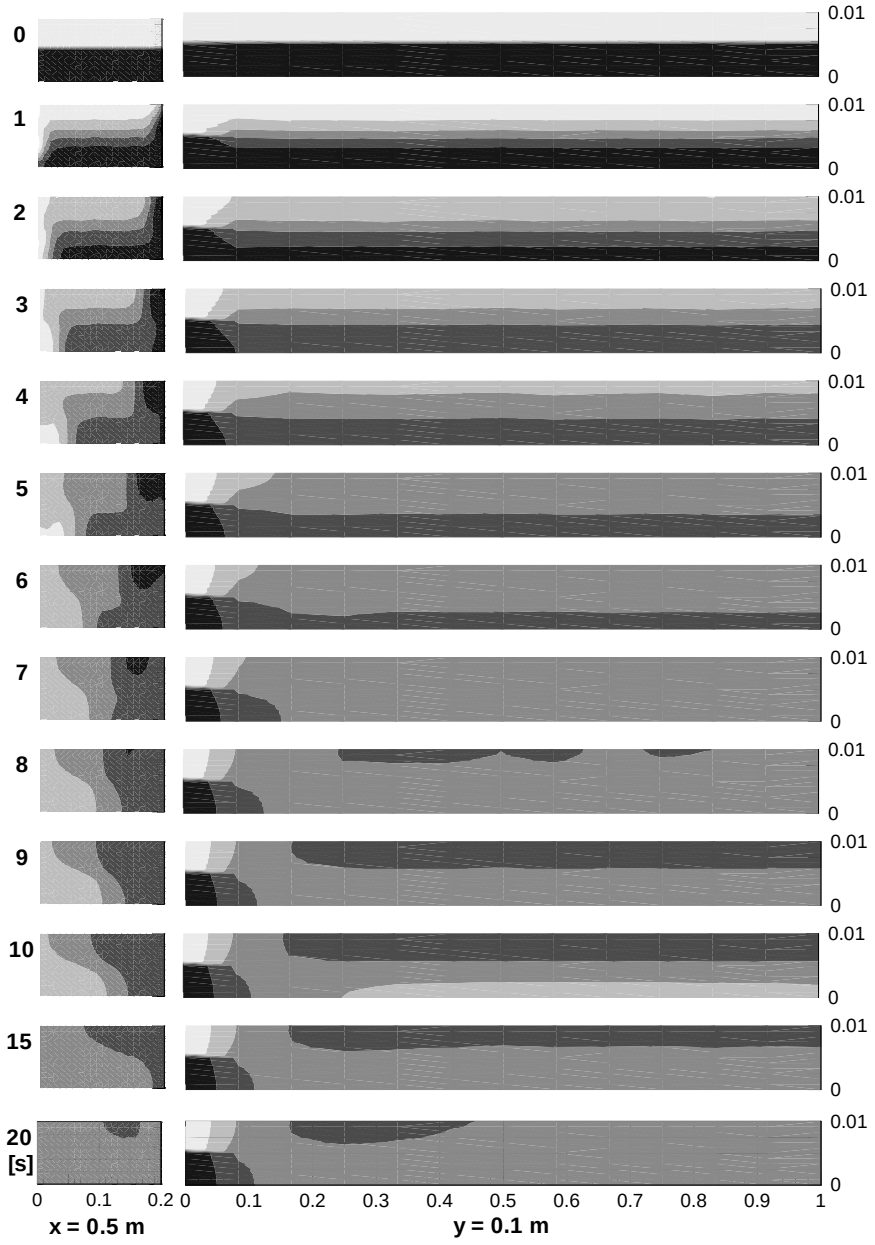

Figure 5.7: Cross-sections of the relative conversion degree for $y = 0.1\,\mathrm{m}$ and $x = 0.5\,\mathrm{m}$ at different times from 0 to 20 s (from 0.25 : dark gray, to 0.75 : light gray). All L_{ijkl} coefficients are 0 except $L_{\perp\parallel} = 0.17\,\mathrm{mm}$.

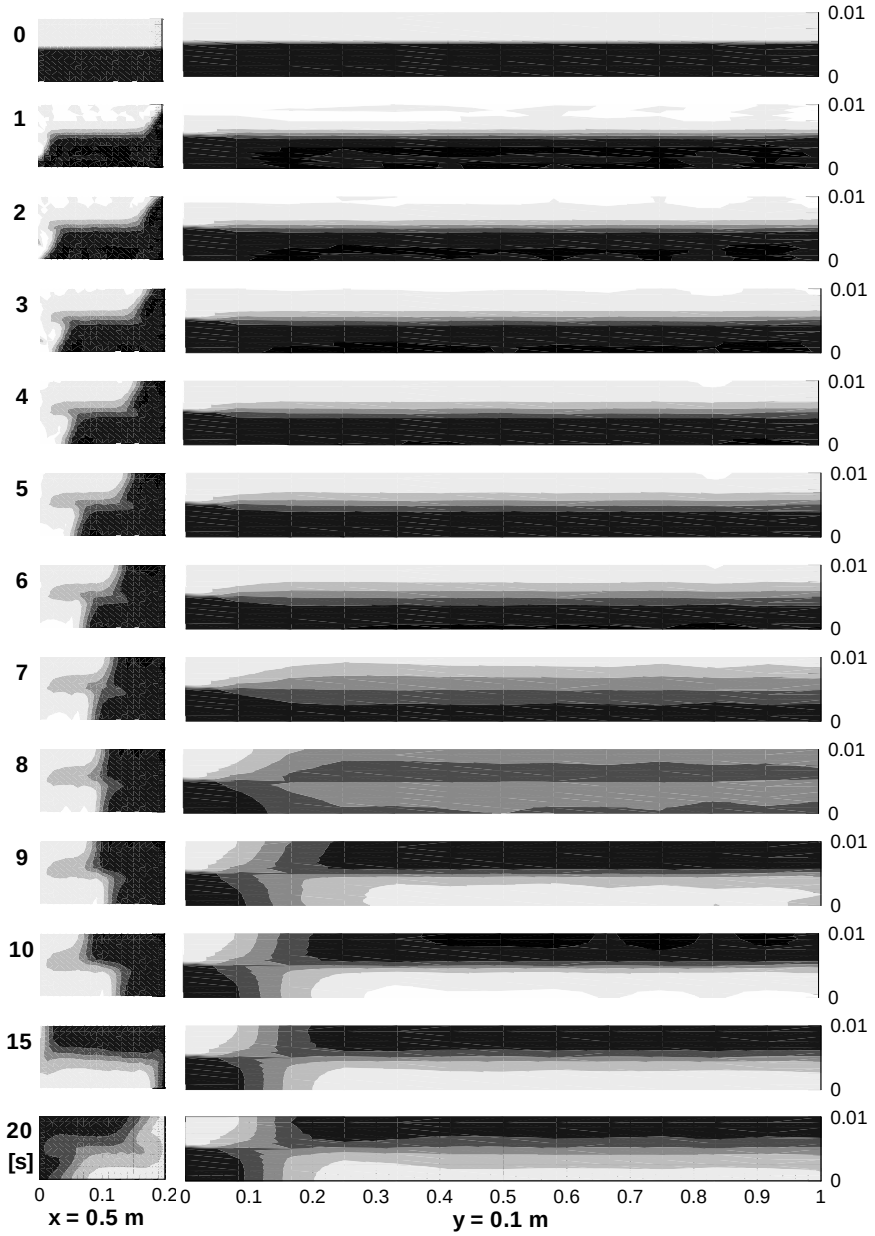

Figure 5.8: Same as Fig.5.7 with $L_{\perp\|} = 0.017\,\text{mm}$.

version (or the rate of conversion) will become the single thermodynamical variable of our model to represent the resin composition.

As it was explained when establishing model (1.9.106), constitutive equations are needed in order to deal with reactive processes. Hence, reaction kinetics and viscosity are here expressed, as a function of temperature and conversion rate (Section 1.8). Although they could have an important effect in some particular cases (53; 55; 33), the heat flux, the specific mass and specific internal energy dependence with respect to the same thermodynamical variables are nevertheless neglected and in this work the related constitutive equations are not developed.

5.3.1 Reaction Kinetics

It can be observed that the chemical reactions related to injection molding processes are mostly exothermic. Intuitively, the amount of heat liberated by the reaction should then be a pertinent indicator of the conversion degree. This heat can be measured by different methods and the shape of the function $f_c(\cdot)$ in Eq. (5.3.39) can be determined by this way. A typical evolution of the degree of conversion observed under isothermal operating conditions for an unsaturated polyester resin is given in Fig. 5.9.

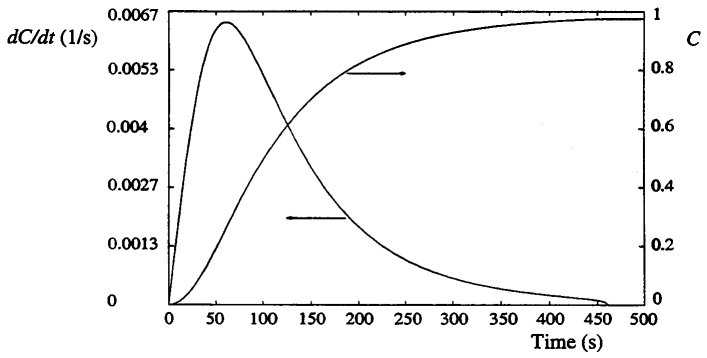

Figure 5.9: Typical evolution of the degree of conversion under isothermal operating conditions for an unsaturated polyester (4).

Whereas the degree of conversion evolves monotonically, its rate of change increases before decreasing up to vanishing when the reaction is almost completed. Simple n^{th}-order kinetic models cannot reproduce this behaviour. On the contrary, the empir-

ical model of Kamal and Sourour (29) has proved to be relevant for a wide range of autocatalytic materials :

$$f_c(c,T) = (k_1 + k_2 c^m)(1-c)^n \quad \text{with} \quad k_i = k_{i0} exp\left(-\frac{E_i}{RT}\right). \tag{5.3.40}$$

This law shows to well fit the degree of conversion evolution in many cases. There exists however other approaches, such as the semi-mechanistic model developed by Stevenson (30), which are more accurate and above all more practical when the resin formulation is changed. This last approach is not investigated in our study.

In our model, the degree of conversion is defined by its intrinsic phase average, and the same approach is used for temperature. The kinetics has an important influence on the conversion degree and temperature evolution. Therefore, the evolution of the temperature field taking into account the effect of the reaction kinetics has been analyzed and the results is shown in Fig. 5.10, where a cold resin injected in a hot mold whose sides are kept hot. Typical values of the material parameters for a polyurethane resin are $k_{10} = 93.6\ 10^6\ 1/\text{s}$, $k_{20} = 0\ 1/\text{s}$, $E_1 = 57800$ J/Mol, $E_2 = 0$ J/Mol, $m = 0.0$ and $n = 2.0$ (56).

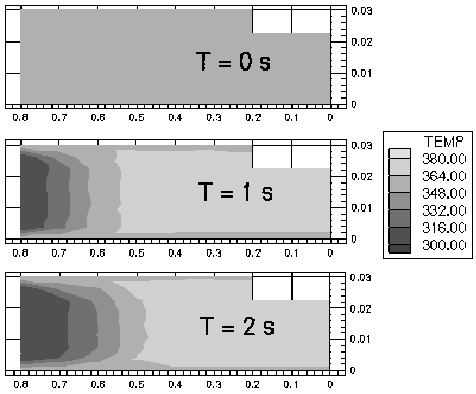

Figure 5.10: Evolution of the temperature field when a cold polyurethane resin fills an initially hot medium (5).

5.3.2 Viscosity

Even if the presence of the fiber reinforcement in RTM and SRIM processes induces a non-Newtonian behaviour of the resin (54), this effect as well as the pressure influence on viscosity were neglected in this study. On the contrary, the important effects of the conversion degree and the temperature on the viscosity are taken into account. Indeed, on the one hand, the more the resin has reacted, the longer the polymer chains are. This effect induces an increase of the resin viscosity during curing, which reaches its maximum when the degree of conversion reaches the **gel point** defined as C_g. This point is indeed referred to as the conversion degree value where the resin becomes unable to flow (its viscosity therefore tends to infinity). On the other hand, at a constant value of the conversion degree, the hotter the resin, the lower the viscosity. This effect is here taken into account by a simple Arrhenius law. The following model combines both phenomena :

$$\eta = \left(\frac{C_g}{C_g - c}\right)^{\alpha_1+\alpha_2 c} A_\eta \exp\left(\frac{E_\mu}{RT}\right). \tag{5.3.41}$$

The numerical results shown in Fig. 5.10 have been performed using this model and with $A_\eta = 4.1\ 10^{-8}$ Pa s, $E_\eta = 38300$ J/Mol, $\alpha_1 = 4.0$, $\alpha_2 = -2.0$ and $C_g = 0.85$.

5.4 Remark : Thermal and material moving fronts

Another specificity of flows in porous media, and in particular of RTM and SRIM processes, is the existence of different moving fronts, viz. the material and the thermal moving fronts[1]. Indeed, when the fluid flows across the pores, heat is present in both the solid and fluid phases. Heat therefore has to cross two barriers, which results in the fact that the thermal front velocity is lower than the material front velocity. This effect is obviously reproduced by the energy equation (1.6.94) and is due the solid specific heat influence in the non-stationary term. Results in Fig. 5.11 illustrate this effect. A hot fluid is injected into a cold and saturated porous cavity. The fluid velocity is maintained constant (no reaction, constant viscosity) and is such that the fluid spends 1 second to move from the inlet to the outlet. Diffusion effects are negligible. It appears that for the chosen parameters, the thermal moving front moves in the cavity twice slower than the material front.

[1] The thermal moving front is defined by the motion of an iso-thermal curve where steep gradients are observed.

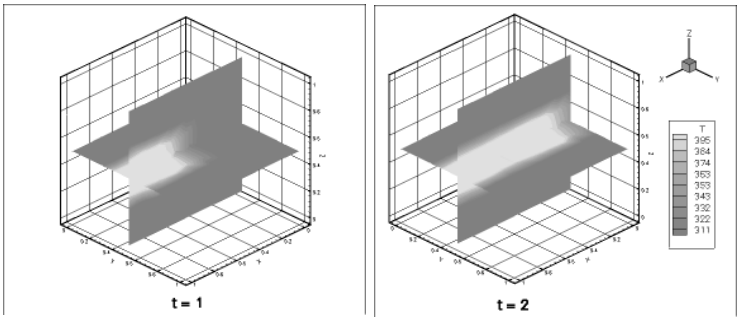

Figure 5.11: Difference between material and thermal fronts. After 1 second, the material front has already reached the cavity extremity, while the thermal front has almost reached the middle of the cavity.